Astronomy & Astrophysics

Hard X-ray variability of V404 Cygni during the 2015 outburst*

C. Sánchez-Fernández[1], J. J. E. Kajava[1,2,3], S. E. Motta[4], and E. Kuulkers[1,5]

[1] European Space Astronomy Centre (ESA/ESAC), Science Operations Department, 28691 Villanueva de la Cañada, Madrid, Spain
e-mail: Celia.Sanchez@sciops.esa.int
[2] Finnish Centre for Astronomy with ESO (FINCA), University of Turku, Väisäläntie 20, 21500 Piikkiö, Finland
[3] Tuorla Observatory, Department of Physics and Astronomy, University of Turku, Väisäläntie 20, 21500 Piikkiö, Finland
[4] University of Oxford, Department of Physics, Astrophysics, Denys Wilkinson Building, Keble Road, Oxford OX1 3RH, UK
[5] ESA/ESTEC, Keplerlaan 1, 2201 AZ Noordwijk, The Netherlands

ABSTRACT

Aims. Hard X-ray spectra of black hole binaries (BHB) are produced by Comptonization of soft seed photons by hot electrons near the black hole. The slope of the resulting energy spectra is governed by two main parameters: the electron temperature (T_e) and optical depth (τ) of the emitting plasma. Given the extreme brightness of V404 Cyg during the 2015 outburst, we aim to constrain the source spectral properties using an unprecedented time resolution in hard X-rays, and to monitor the evolution of T_e and τ over the outburst.
Methods. We have extracted and analysed 602 X-ray spectra of V404 Cyg obtained by the IBIS/ISGRI instrument on-board INTEGRAL during the 2015 June outburst, using effective integration times ranging between 8 and 176 000 s. We fitted the resulting spectra in the 20–200 keV energy range.
Results. We find that while the light curve and soft X-ray spectra of V404 Cyg are remarkably different from those of other BHBs, the spectral evolution of V404 Cyg in hard X-rays and the relations between the spectral parameters are consistent with those observed in other BHBs. We identify a hard branch in which the T_e is anti-correlated with the hard X-ray flux, and a soft flaring branch in which the relation reverses. In addition, we find that during long X-ray plateaus detected at intermediate fluxes, the thermal Comptonization models fail to describe the spectra. However, the statistics improve if we allow N_H to vary freely in the fits to these spectra.
Conclusions. We conclude that the hard branch in V404 Cyg is analogous to the canonical hard state of BHBs. V404 Cyg never seems to enter the canonical soft state, although the soft flaring branch bears resemblance to the BHB intermediate state and ultra-luminous state. The X-ray plateaus are likely the result of absorption by a Compton-thick outflow ($N_H \gtrsim 10^{24}$ cm^{-2}) which reduces the observed flux by a factor of about 10. Variable covering of the central source by this Compton-thick material may be the reason for the complicated light curve variability, rather than intrinsic source variability.

Key words. accretion, accretion disks – black hole physics – X-rays: binaries – X-rays: individuals: V404 Cyg

1. Introduction

Black hole (BH) binary systems (BHBs) can go through various spectral states that are thought to be caused by changes in the accretion geometry and accretion rates close to the BH, although the actual details still remain debated (Remillard & McClintock 2006; Belloni & Motta 2016). The two most common states are the hard and the soft states (see, e.g., Done et al. 2007; Poutanen & Veledina 2014, for review). In the hard state, the spectrum can be described by a power law with a variable cut-off energy around 60–150 keV, which is thought to result from Comptonization of soft seed photons by a population of hot electrons located in an optically thin region close to the BH (Shapiro et al. 1976; Narayan & Yi 1995). The high energy cut-off suggests a thermal distribution of electrons with temperatures in the range 30–100 keV (Sunyaev & Truemper 1979; Gierliński et al. 1999). Occasionally, a hard excess has been observed above 100 keV which suggests the presence of non-thermal electrons as well (see e.g. McConnell et al. 2002; Wardziński et al. 2002; Joinet et al. 2007; Droulans et al. 2010) either in the corona/hot flow or in the base of the jet (e.g.,

Zdziarski et al. 2012). In the soft state, thermal emission peaking at ~1 keV, from a cool, optically thick, geometrically thin accretion disk dominates the spectrum (Shakura & Sunyaev 1973; Esin et al. 1997). A weak, hard X-ray tail extending up to the MeV range is also detected (Zdziarski et al. 2017). This tail is thought to originate from Comptonized emission by non-thermal electrons in discrete flares on top of the accretion disk (McConnell et al. 2002). During transitions between the hard and soft states, BHBs pass through additional intermediate states, which show characteristic features of both (see e.g. Ebisawa et al. 1994; Malzac et al. 2006; Belloni & Motta 2016). On rare occasions, some systems may pass also through the so-called ultra-luminous state (Motta et al. 2012), which is also called the very high state or anomalous state; this is an intermediate state characterized by both a strong thermal component and a very strong and steep hard X-ray tail (Done et al. 2007).

One of the current observational challenges in this context is to determine the electron temperature, T_e, and optical depth, τ, of the Comptonizing medium. These together determine the spectral slope of the Comptonized spectrum (e.g. Beloborodov 1999). Because the cut-off energies are found around 100 keV, where usually the instrumental response is low, observations sensitive enough to constrain these parameters have only been available for a few sources and typically require long exposures. Observations in the hard state of GRO J0422+32 (Esin et al. 1998),

GX 339–4 (Wardziński et al. 2002; Motta et al. 2009), XTE J1550–564 (Rodriguez et al. 2003), Cyg X-1 (Del Santo et al. 2013) and Swift J1753.5–0127 (Kajava et al. 2016) show an anti-correlation between the electron temperature, T_e (or high energy cut-off) and the X-ray flux, accompanied by a correlation between the plasma optical depth, τ, and the X-ray flux (Wardziński et al. 2002). These relations reverse during the hard to soft state transitions. Observations of these transitions in Cyg X-1 (Phlips et al. 1996; Del Santo et al. 2013), GRO J1719–24 (Esin et al. 1998), GRO J1655–40 (Joinet et al. 2008) and GX 339–4 (Motta et al. 2009) show an increasing T_e with increasing flux, while the optical depth τ decreases (Joinet et al. 2008; Del Santo et al. 2013). The cut-off is significantly present during the hard and intermediate states, and it disappears when the source reaches the soft state.

The extremely bright outburst of V404 Cyg in June 2015 provides a unique data set to perform high time-resolved spectroscopy in high energies and study in detail the evolution of the parameters describing the Comptonizing plasma. We present here the results of spectral analysis of IBIS/ISGRI data in the 20–200 keV energy range over the period 18–28 June 2015, when the source was brightest.

V404 Cyg is a transient low-mass X-ray binary (LMXB) consisting of a $9.0^{+0.2}_{-0.6}\,M_\odot$ BH accreting mass from a K3 III companion (Khargharia et al. 2010) in a 6.5 d orbit (Casares et al. 1992). It is located at a distance $d = 2.39 \pm 0.14$ kpc (Miller-Jones et al. 2009). V404 Cyg was first detected in optical wavelengths during two outbursts in 1938 and 1956 (Richter 1989) and later in X-rays during a third outburst in 1989 (Makino 1989; Marsden 1989). The 1989 outburst was characterized by extreme flaring activity, several flux levels above the Crab (Tanaka 1989; Oosterbroek et al. 1996). After ~26 yr in quiescence, the onset of a new outburst was detected by *Swift*/BAT, MAXI and *Fermi*/GBM on 15 June 2015 (Barthelmy & Sbarufatti 2015; Negoro et al. 2015; Younes 2015). This outburst, which triggered the most intensive multiwavelength observing campaign performed so far on a transient BHB, lasted until early August 2015 (Sivakoff et al. 2015). During the first 10 days, the source exhibited violent flaring activity on timescales of subseconds to hours in all wavelengths: γ-rays (Loh et al. 2016) X-rays (Rodriguez et al. 2015; Roques et al. 2015; Jenke et al. 2016; Walton et al. 2016), optical (Gandhi et al. 2016; Kimura et al. 2016; Muñoz-Darias et al. 2016), infrared (Eikenberry et al. 2016) and millimeter/submillimeter and radio (Tetarenko et al. 2015). In some major flares, V404 Cyg reached fluxes around 50 and 40 Crab in soft and hard X-rays, respectively (Segreto et al. 2015; Rodriguez et al. 2015). The peak of the outburst was reached on 26 June, and the flux dropped immediately afterwards (Ferrigno et al. 2015; Walton et al. 2015) slowly fading to quiescence over the subsequent weeks (Sivakoff et al. 2015).

2. Observations and data analysis

V404 Cyg was observed by INTEGRAL, the INTErnational Gamma-Ray Astrophysics Laboratory (Winkler et al. 2003) in a series of Target of Opportunity observations scheduled between 17 June 2015 and 13 July 2015 (MJD 57 556–57 582; revolutions 1554–1563; Kuulkers 2015). We present here the analysis of the available IBIS/ISGRI data (Lebrun et al. 2003), obtained during revolutions 1554–1558 (18–28 June 2015; MJD 57 191–51 201), which cover the epoch of intense flaring activity and the beginning of the outburst decay. These observations provide

data sensitive enough to study in detail the properties of the Comptonizing medium.

2.1. Data reduction

The IBIS/ISGRI data reduction was performed with the Offline Scientific Analysis software (OSA; Courvoisier et al. 2003) v10.2, using the latest calibration files. The data were processed following standard IBIS/ISGRI reduction procedures.

The spectral extraction was performed using good time interval files (GTIs) of variable duration, which are defined to provide source spectra of comparable S/N regardless of the source flux. The GTI selection was based on the source light curves distributed by the INTEGRAL Science Data Center (ISDC; Kuulkers 2015). The GTIs were defined sequentially, and their start/end times were selected such that during each time interval 4×10^5 counts were accumulated in the IBIS/ISGRI 25–60 keV band. This GTI selection was found to be an optimal compromise between time resolution and the ability to constrain the T_e values, particularly for the softer spectra in the sample. Using this strategy, we extracted 602 spectra, with effective exposure times in the range 8 to 176 000 s. We binned the IBIS/ISGRI response matrix in the energy range 20–500 keV using 28 channels of variable logarithmic widths. We restricted the spectral fits to the 20–200 keV energy range to remove potential background contamination, and the contribution of additional spectral components above 200 keV, such as hard non-thermal tails (Rodriguez et al. 2015; Roques et al. 2015) or hard X-ray emission caused by positron annihilation (Siegert et al. 2016). In our fits we ignored the energy bin around 50 keV due to calibration uncertainties and added 3 per cent systematic errors to the spectral bins. The IBIS/ISGRI X-ray spectra were fit via XSPEC v12.8.2 (Arnaud 1996), adopting the χ^2 statistics. Errors provided below are quoted at the 1σ confidence level ($\Delta\chi^2 = 1$ for one parameter of interest).

2.2. Spectral modelling

We show in Fig. 1 a sample of the IBIS/ISGRI spectra of V404 Cyg analysed in this work. On most occasions, the spectra have a shape that is power-law like, modified by a cut-off at high energies, which is consistent with a thermal Comptonization spectrum (see Fig. 1a). Therefore, we used Comptonization models to fit our data: NTHCOMP (Zdziarski et al. 1996; Życki et al. 1999) and COMPPS (Poutanen & Svensson 1996). These models provide a description of the continuum produced by thermal Compton up-scattering of soft X-ray photons. The NTHCOMP model is parameterized by a power-law index Γ and an electron temperature T_e. The COMPPS parameters are the electron temperature T_e and optical depth τ. Although a thermal component was never detected during the June 2015 outburst (Motta et al., in prep.), in our fits we fixed the seed photon temperature $T_{bb} = 0.1$ keV, as fits by Motta et al. (2017) to the source spectra over the 0.6–200 keV energy range, with Comptonization models are consistent with this value.

In some cases, a high-energy cut-off is either weakly significant or not statistically required by the data (see Fig. 1b). These spectra can still be fit using Comptonization models, but fixing T_e to an arbitrary high value ($T_e = 999$ keV). To account for both possibilities, we carried out two independent fitting runs per model. In the first fitting run, we fit every spectrum leaving T_e as a free parameter, while in the second fitting run we fixed it to $T_e = 999$ keV. Then, the Bayesian information criterion (BIC;
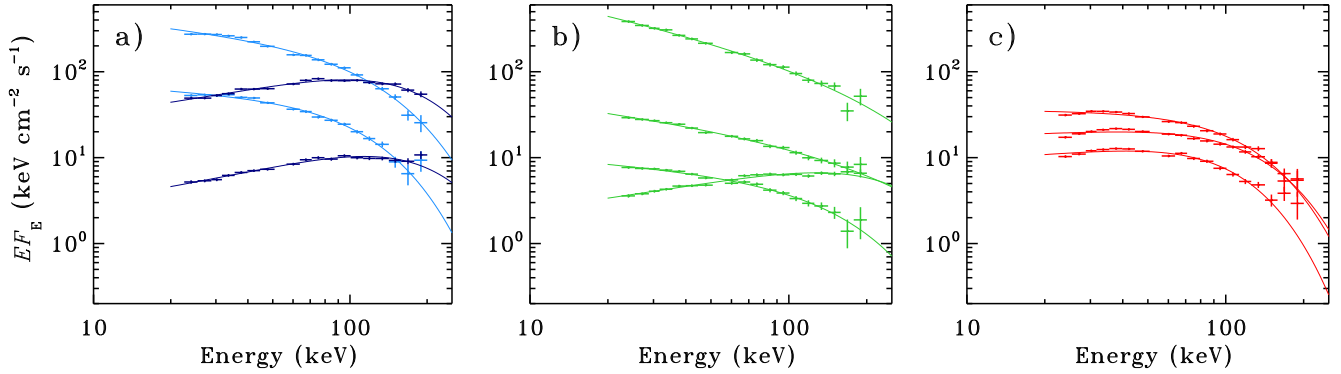
Fig. 1. Example of the spectra analysed in this work. Panel **a)** Comptonized spectra showing a cut-off at high energies within the IBIS/ISGRI energy range. We classify these spectra in two groups: *hard* ($\Gamma \leq 1.7$; dark blue) and *soft* ($\Gamma > 1.7$; light blue). The hardness selection is based on the Γ values derived using the NTHCOMP model. From top to bottom, the effective integration times for these spectra are 36, 170 s ($\Gamma > 1.7$ spectra) and 91, 1285 s ($\Gamma \leq 1.7$ spectra). Panel **b)** Comptonized spectra for which T_e cannot be constrained by our data. We fixed the electron temperature to the value $T_e = 999$ keV in these spectral fits. We note the range in fluxes and hardness presented by these spectra. The effective integration times for these spectra are 8, 403, 1730 and 2251 s (top to bottom). Panel **c)** spectra for which a Comptonized model was not statistically favoured by our model selection criteria (p–value <0.05). These spectra are predominantly found during the X-ray plateaus detected at fluxes $F_x \sim 5 \times 10^{-8}$ erg cm^{-2} s^{-1}, as explained in the text. The effective integration times for these spectra are 297, 579 and 912 s (top to bottom).

Schwarz 1978) was independently applied to the results obtained for every spectrum, to select the best fit to the data. We computed the BIC with the following approximation: BIC $= \chi^2 + k \ln(n)$, where k is the number of parameters in the model, and n is the number of channels in the spectral fits. In a model selection process, the optimal model is identified by the minimum value of BIC. A lower BIC implies either fewer explanatory variables, a better fit, or both. Kass (1995) set the strength of the evidence against the model with the higher BIC to be strong if ΔBIC > 6, which we adopted as the limit for model selection. This approach was applied to the NTHCOMP and COMPPS fits. The results of this analysis are described in Sects. 3.1–3.3, and shown in Figs. 2–A.3. In these figures the data are presented according to the following colour convention:

– Blue points are used to highlight those fits where the ΔBIC model selection favoured a Comptonization model with a constrained electron temperature T_e, further divided in two groups: hard spectra ($\Gamma \leq 1.7$; dark blue) and soft spectra ($\Gamma > 1.7$; light blue). Some of these spectra are shown in Fig. 1a. The latter classification is based on the Γ values derived from the NTHCOMP fits, and then applied to the COMPPS fits.
– Green points correspond to those spectra where T_e could not be constrained by our fits (i.e. T_e fixed at 999 keV). Some of these spectra are shown in Fig. 1b.
– Additionally, we computed the corresponding p–value of the fit with respect to the data for every fit. We mark the spectra where $p < 0.05$ with red symbols. Some of these spectra are shown in Fig. 1c.

To improve the fits to the latter group of spectra, we also explored the possibility that these were affected by heavy absorption. The results of these additional fits are presented in Sect. 3.4.

3. Results

3.1. Parameter evolution

We present in Fig. 2 the time evolution of the source flux computed in the 20–200 keV energy range, together with the evolution of the spectral parameters derived using NTHCOMP (Γ, T_e) and COMPPS (τ, T_e) and the corresponding χ^2_ν values.

Hereafter we refer to the flux in the 20–200 keV energy range as F_x.

3.1.1. EPOCH 1: flaring activity

During the period MJD 57 191–57 193 (Rev. 1554; EPOCH 1 in Fig. 2a) intense flaring activity was detected on timescales of minutes to hours. The flares reached peak fluxes of $F_x \sim 55 \times 10^{-8}$ erg cm^{-2} s^{-1}, while between flares we measure fluxes below $F_x \sim 2 \times 10^{-8}$ erg cm^{-2} s^{-1}. Over this period, the source spectrum was hard ($\Gamma \leq 1.7$) and only softened when F_x increased above $\gtrsim 25 \times 10^{-8}$ erg cm^{-2} s^{-1} (i.e. during the peaks of the flares). The value T_e is well constrained during the X-ray flares with values in the range 30–100 keV (NTHCOMP) or 30–70 keV (COMPPS). Between flares T_e cannot be constrained in our spectral fits and the X-ray spectrum is consistent with a hard power law ($\Gamma \leq 1.7$) with no cut-off (see Fig. 1b). Similar results were obtained by Natalucci et al. (2015), who analysed this data set using a different time resolution, and Roques et al. (2015), who analysed contemporaneous INTEGRAL/SPI data.

In EPOCH 1 τ varied between 2 and 5. It displayed higher values ($\tau \gtrsim 3.5$) when the spectrum was hard ($\Gamma \leq 1.7$) and decreased ($\tau \lesssim 3.5$) as the spectrum softened ($\Gamma > 1.7$; see Fig. 2d).

3.1.2. EPOCH 2: spectral softening, state transitions, and X-ray plateaus

During the intervals MJD 57 193.5–57 195.5 and MJD 57 196.7–57 197.4 (Rev. 1555–1556; EPOCH 2 in Fig. 2a) the flaring activity persisted. Peak fluxes of $F_p \sim 60$–80×10^{-8} erg cm^{-2} s^{-1} were measured. Between flares, we find again fluxes $F_x \lesssim 2 \times 10^{-8}$ erg cm^{-2} s^{-1}. In general, in EPOCH 2 V404 Cyg displayed softer spectra than during EPOCH 1 even at the lowest count rates, when spectra with $\Gamma \sim 2.3$ without a cut-off were frequently observed. Only one of the X-ray flares (detected around MJD 57 195.15) displayed a hard X-ray spectrum ($\Gamma \leq 1.7$). Several transitions between Comptonized hard ($\Gamma \leq 1.7$) and soft ($\Gamma \sim 3$) spectra with unconstrained T_e occurred.

In EPOCH 2, there is more scatter in the measured T_e, τ and Γ parameters than in EPOCH 1. Also, the relation between F_x and Γ is complex: while during some flares Γ was roughly
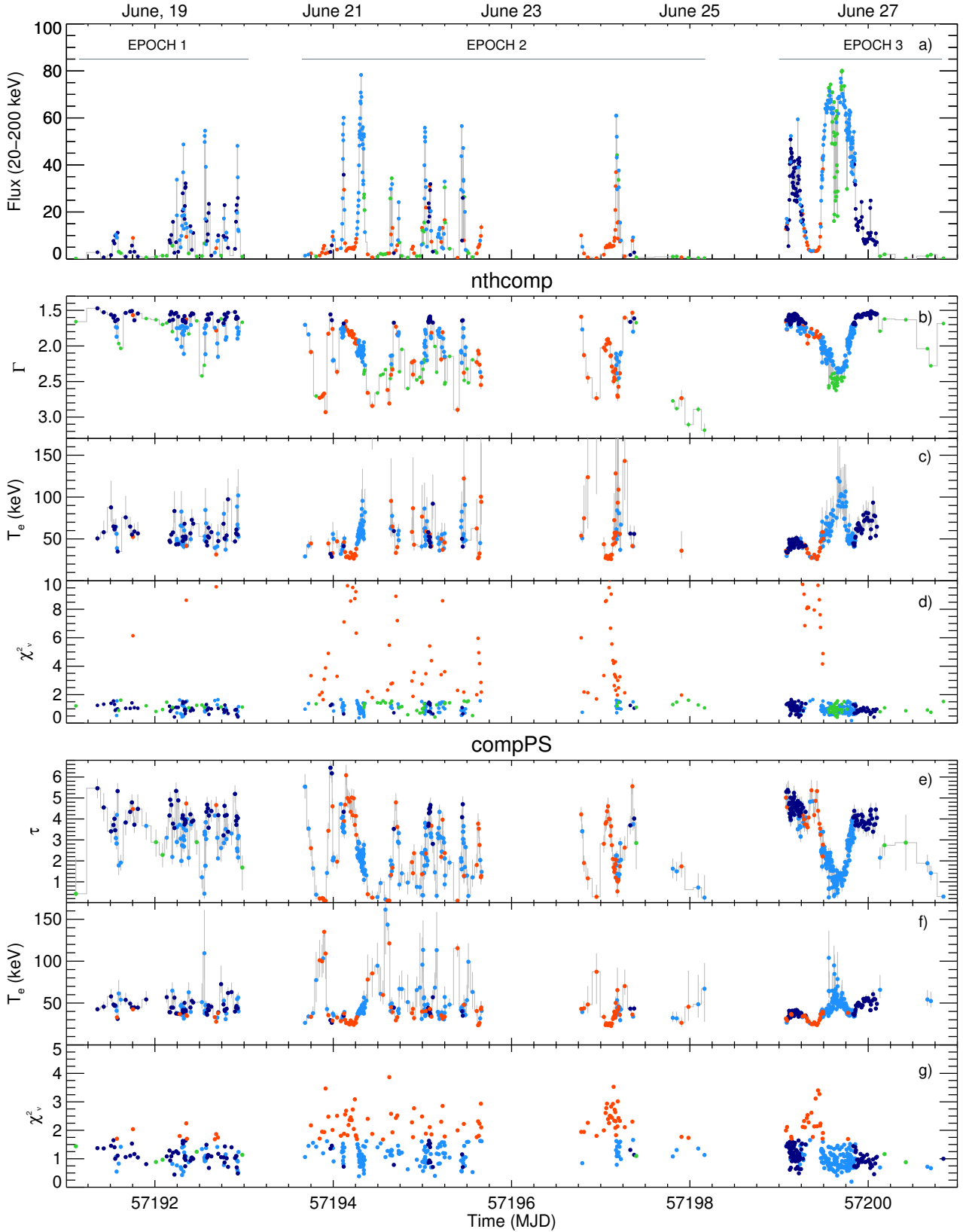
Fig. 2. Evolution of the flux and spectral parameters of V404 Cyg during the June 2015 flaring episodes. Panel **a)** source flux (20–200 keV) in units of 10^{-8} erg cm^{-2} s^{-1}. Panels **b)**, **c)**, **d)** NTHCOMP fitting parameters (power-law index, Γ, electron temperature, T_e and χ^2_ν). Panels **e)**, **f)**, **g)** COMPPS fitting parameters (optical depth, τ, electron temperature, T_e and χ^2_ν). Green, blue and red symbols are used to highlight the best-fitting model, according to our model selection criteria (Sect. 2.2). Blue: comptonization models with constrained T_e (Fig. 1a) further divided into hard ($\Gamma \leq 1.7$; dark blue) and soft spectra ($\Gamma > 1.7$; light blue). Green: comptonization models with unconstrained T_e (Fig. 1b). Red: comptonization models with p–value <0.05 fits. (Fig. 1c); $\chi^2_\nu \gtrsim 2$ values are only obtained during the X-ray plateaus observed at $F_x \sim 5 \times 10^{-8}$ erg cm^{-2} s^{-1}.

constant (e.g. flare on MJD 57 194.10, Fig. A.1), in other flares the spectrum hardened (e.g. flare on MJD 57 195.5) or softened during the entire flare (e.g. flare on MJD 57 194.3, Fig. A.1). During the flares, T_e displayed values in the range 30–120 keV (NTHCOMP) or 20–150 keV (COMPPS). Very soft spectra ($\Gamma \sim 3$) with unconstrained T_e were detected by the end of EPOCH 2, when the flux dropped below $\sim 2 \times 10^{-8}$ erg cm^{-2} s^{-1}.

One additional feature over this period is the detection of X-ray plateaus (i.e. non-varying flux periods) at intermediate fluxes ($F_x \sim 5 \times 10^{-8}$ erg cm^{-2} s^{-1}). These plateaus last several hours and happen in between successive X-ray flares (red points in Fig. 2; see also Rodriguez et al. 2015). For a closer view of one of these plateaus see Fig. A.1. We consistently obtain p–values < 0.05 and $\chi^2_\nu > 1.8$ when modelling the plateau spectra using Comptonization models (NTHCOMP or COMPPS), which also provide systematically lower electron temperatures for these data points ($T_e \sim 30$ keV) than those derived in fits to contemporaneous flare spectra ($T_e \sim 50$ keV). Joint spectral fits to simultaneous *Swift*/XRT, INTEGRAL/JEMX and INTEGRAL/ISGRI data by Motta et al. (2017) obtained during the plateau observed on MJD 57 194, showed a high absorption ($N_H \approx 1.4 \times 10^{24}$ cm^{-2}) over a dominant reflection component.

Adding an absorption component (TBABS; $N_H \gtrsim 10^{24}$ cm^{-2}) to the fits to the plateau spectra (as described in detail in Sect. 3.4), we obtain $T_e \sim 50$ keV, in better agreement with the values derived during contemporaneous flares.

3.1.3. EPOCH 3: major flares and onset of outburst decay

Between MJD 57 199.05 and MJD 57 200.10 we observed two major flares separated by a long X-ray plateau, similar to those seen in EPOCH 2. The first flare (MJD 57 199.05–57 199.15; Fig. A.2) reached a peak flux $F_x \sim 55 \times 10^{-8}$ erg cm^{-2} s^{-1}. During this flare, the spectrum was hard ($\Gamma \leq 1.7$), contrary to the softer flares detected in EPOCH 2. We measure roughly constant electron temperatures ($T_e \sim 50$ keV) and an optical depth τ in the range [4–5.5], which decreased as the flare proceeded. During the subsequent X-ray plateau a flux $F_x \sim 5 \times 10^{-8}$ erg cm^{-2} s^{-1} was measured (Fig. A.2). The plateau lasted ~ 0.15 day.

The plateau was followed by a major X-ray flare (MJD 57 199.50–57 199.80; Fig. A.3) during which the source reached the highest fluxes measured during the 2015 outburst ($F_x \sim 80 \times 10^{-8}$ erg cm^{-2} s^{-1}). The flare had two peaks separated by a ~ 1 h drop in flux (from ~ 70 to $\sim 20 \times 10^{-8}$ erg cm^{-2} s^{-1} and back to $\sim 80 \times 10^{-8}$ erg cm^{-2} s^{-1}). Over the flare rise and decay we find a Comptonized, soft, X-ray spectrum that softened as F_x increased and hardened as F_x decreased. The value T_e also evolved in correlation with the flux variations and reached values above ~ 130 keV (NTHCOMP) or ~ 90 keV (COMPPS) during the peak of the flare. On some occasions around the peak of the flare T_e is not constrained by our fits (NTHCOMP).

During the flare decay we find an abrupt drop in flux (from ~ 45 to $\sim 15 \times 10^{-8}$ erg cm^{-2} s^{-1}), which happened in less than half an hour. The drop in flux was accompanied by a transition to harder spectra, characterized by a roughly constant power-law index ($\Gamma \gtrsim 1.5$), increasing T_e and decreasing τ. After the transition, the flux decay continued at a roughly constant Γ. As the flux evolved towards quiescence values, the spectrum softened again, T_e was unconstrained and the optical depth, τ, decreased. The two lowest flux spectra in Fig. 1b correspond to this period.

3.2. Parameter distributions

The distributions of the spectral parameters derived in this analysis are shown in Fig. 3. The integration times of the spectra are flux dependent, and consequently the parameter distributions are skewed towards higher fluxes when the integration times are shorter and therefore the sampling is more frequent.

The F_x distribution is shown in Figs. 3a and d. We measure fluxes in the range $[0.01–80] \times 10^{-8}$ erg cm^{-2} s^{-1} with a peak in the distribution at $\sim 50 \times 10^{-8}$ erg cm^{-2} s^{-1}. We do not find hard Comptonized spectra ($\Gamma \leq 1.7$) when $F_x \gtrsim 50 \times 10^{-8}$ erg cm^{-2} s^{-1}. We find soft Comptonized spectra ($\Gamma > 1.7$) for fluxes in the range $[4–80]$ ($\times 10^{-8}$ erg cm^{-2} s^{-1}). Comptonized spectra with unconstrained electron temperatures are predominantly found at the lowest and highest fluxes. Spectra not compatible with Comptonized models are predominant in the range of fluxes $[1.5–6] \times 10^{-8}$ erg cm^{-2} s^{-1}, with a peak in the distribution at 5×10^{-8} erg cm^{-2} s^{-1}.

The photon index (Γ; Fig. 3b) was derived using the NTHCOMP model. The distribution of Γ values is asymmetric with a peak at $\Gamma \sim 1.7$ and a tail extending to $\Gamma \sim 3.0$. We measure Γ values in the range [1.5–2.4] for the Comptonized spectra with constrained T_e. All the Comptonized spectra softer than $\Gamma \gtrsim 2.4$ display unconstrained T_e in our NTHCOMP fits. There are also a fraction of hard spectra ($\Gamma \sim 1.7$) with unconstrained T_e. The spectra detected during X-ray plateaus display Γ values in the range [1.6–3.0] with a peak in the distribution at $\Gamma = 1.8$.

The optical depth of the Comptonizing plasma (τ; Fig. 3e), which is derived via COMPPS shows a large scatter in values, in the range [0.1−5.0]. The hard and soft spectra have different τ distributions. For the hard spectra ($\Gamma \leq 1.7$) we derive τ values in the range [3–5.5]. For the softer spectra ($1.7 < \Gamma \leq 2.4$), we derive τ values in the range [0.1–4.5].

The electron temperatures that we derive via the NTHCOMP and COMPPS models (Figs. 3c and f) display similar distributions with a narrow peak at moderate temperatures (NTHCOMP: 45 keV; COMPPS: 35 keV) and a tail extending up to ~ 150 keV. However, the distribution of T_e derived using NTHCOMP is broader than the distribution of values obtained from the COMPPS fits. We find more spectra with unconstrained T_e using NTHCOMP than using COMPPS, which is probably because of the systematically lower T_e values derived using COMPPS. The electron temperatures derived for Comptonized hard ($\Gamma \leq 1.7$) and soft spectra ($\Gamma > 1.7$) have consistent values, but we note that the tail of the T_e distribution extends to higher energies for the soft Comptonized spectra than for the hard spectra. The fits to the spectra obtained during X-ray plateaus provide a broad T_e distribution, which peaks at lower energies than the T_e distribution derived for the Comptonized spectra (~ 25 keV) and extend up to ~ 130 keV.

3.3. Parameter relations

The flux dependencies of the photon index and optical depth are presented in the $F_x − \Gamma$ and $F_x − \tau$ diagrams (Figs. 4a, d). We find that the hard spectra in our sample ($\Gamma \leq 1.7$) occupy a region in the F_x–Γ diagram that is reminiscent of the hard state in the BHB Hardness-Intensity Diagram (HID; Homan et al. 2001; Belloni 2004; Fender et al. 2004; Dunn et al. 2010). In this region, which we call hereafter the hard branch, the spectrum softens (from $\Gamma \approx 1.5$ to $\Gamma \approx 1.7$) while the flux increases and the optical depth increases with increasing flux from $\tau \sim 3$ to $\tau \sim 5.5$ (Fig. 4d). The hard spectra also occupy defined regions in the F_x–T_e, Γ–T_e, and τ–T_e diagrams (Figs. 4b, e, c, f). In these hard branch(es),
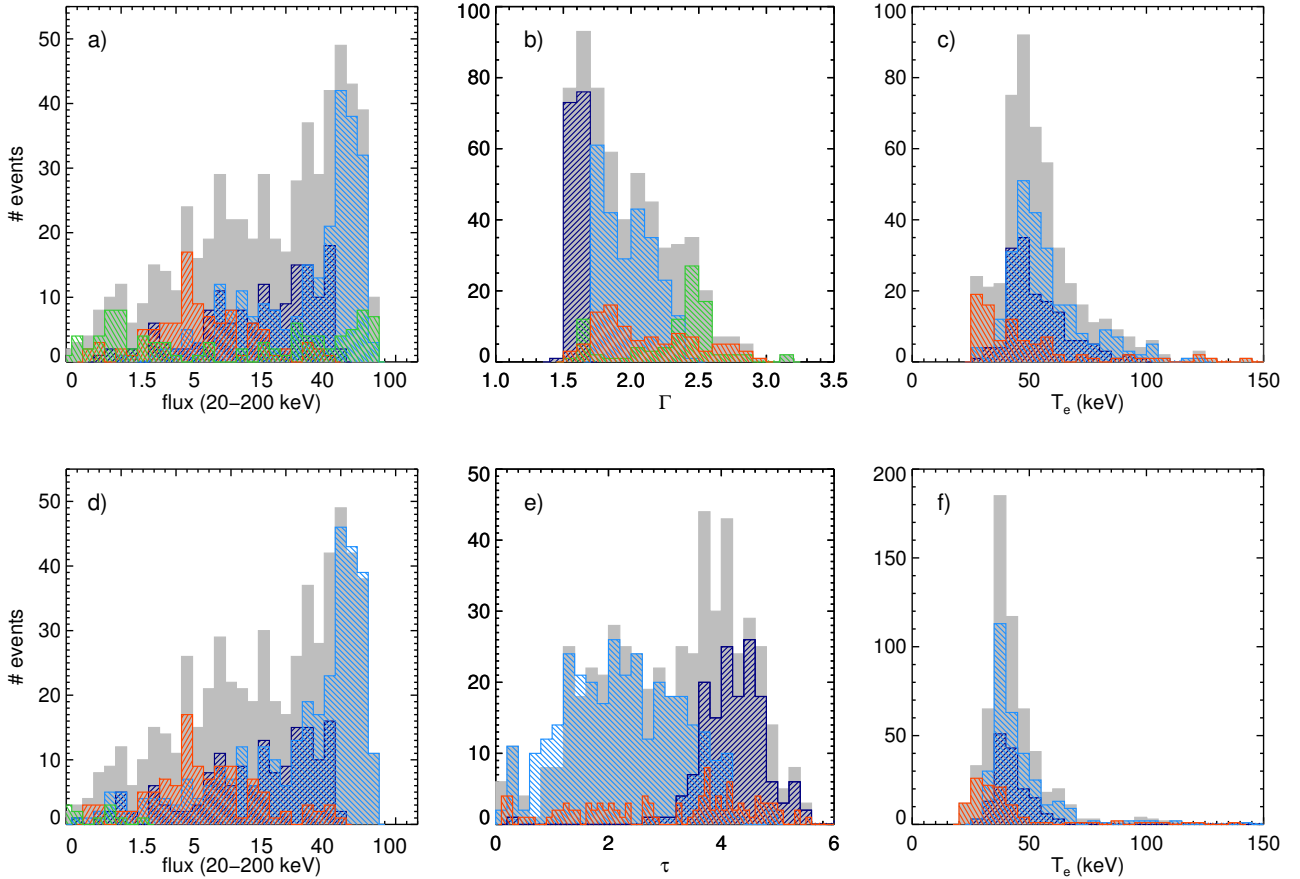
Fig. 3. Distribution of the spectral parameters obtained in the fits to the IBIS/ISGRI spectra of V404 Cyg analysed in this work. Grey bars are used to describe the total parameter distribution. Green, blue, and red symbols are used to highlight the best-fitting model, according to our model selection criteria (Sect. 2.2). Blue: comptonization models with constrained T_e (Fig. 1a) further divided into hard ($\Gamma \leq 1.7$; dark blue) and soft spectra ($\Gamma > 1.7$; light blue). Green: comptonization models with unconstrained T_e (Fig. 1b). Red: p–value <0.05 fits. (Fig. 1c). In *the top panels* we show the distribution of the NTHCOMP parameters, while in the *bottom panels* we show the COMPPS parameters.

T_e is anti-correlated with F_x (Fig. 4b, e). We also find that T_e is anti-correlated with Γ and τ (4c, f).

The soft ($\Gamma > 1.7$) spectra in our sample, detected during the brightest X-ray flares, occupy a distinct region in the $F_x - \Gamma$ diagram (Fig. 4a) which we call hereafter the soft flaring branch. In the soft flaring branch the spectrum still softens as the flux increases (Fig. 4a) even though most of the parameter dependencies are reversed with respect to the hard branch: τ is seen to decrease with increasing flux (Fig. 4d), F_x and T_e are correlated (Fig. 4b, e), and the $\Gamma - T_e$ dependency is also reversed. In the $\tau - T_e$ diagram, we find a range of τ values ($\tau \approx [2.5–4]$) for which T_e displays a roughly constant value (~ 40 keV). Below $\tau \lesssim 2.5$ T_e and τ are anti-correlated (Fig. 4f).

For spectra softer than $\Gamma \gtrsim 2.4$ the spectral fits using NTH-COMP do not provide constrained electron temperatures. These soft spectra are detected at the highest ($\gtrsim 20 \times 10^{-8}$ erg cm^{-2} s^{-1}) and lowest ($\lesssim 2 \times 10^{-8}$ erg cm^{-2} s^{-1}) F_x values. When detected at the highest fluxes, they occupy regions in the $F_x – \Gamma$ diagram (Fig. 4a) that are reminiscent of the HID ultra-luminous state (Motta et al. 2014).

Finally, we also observe that the spectra detected during X-ray plateaus occupy separate regions, in all these diagrams, which are distinct from the Comptonized branches; this confirms our classification of these spectra in a separate category. We call these regions plateau branch(es).

3.4. Fits to the plateau spectra using variable absorption

To study the poor fitting spectra detected during X-ray plateaus, we also considered the possibility that these were the result of obscuration of the primary X-ray emitting region. Absorption by Compton-thick material ($N_H \gtrsim 10^{24}$ cm^{-2}) can substantially reduce the source flux for energies up to ~ 30–40 keV, and also change the spectral slope and produce a global flux reduction by a factor 10 in the 40–300 keV energy range (Murphy & Yaqoob 2009). Joint spectral fits to simultaneous *Swift*/XRT and INTEGRAL/JEMX+ISGRI spectra during the X-ray plateau around MJD 57 195 by Motta et al. (2017) already showed that the broadband spectrum of V404 Cyg around that period was compatible with heavily absorbed Comptonized emission ($N_H \sim 1$–3×10^{24} cm^{-2}) with a prominent scattered component.

For the above reasons, we performed two additional fitting runs using COMPPS. In the first fitting run, we left N_H as a free parameter. The results of these fits are presented in Fig. 5. In the second fitting run we also allowed the Compton reflection amplitude parameter in COMPPS to vary freely. The results obtained in these fits are presented in Fig. 6. In both cases, we compared the results obtained in these fits against those obtained using a model where the absorption was fixed to interstellar values, as described in the previous sections. We computed the BIC for each fit, and again applied the ΔBIC > 6 criterium to select the

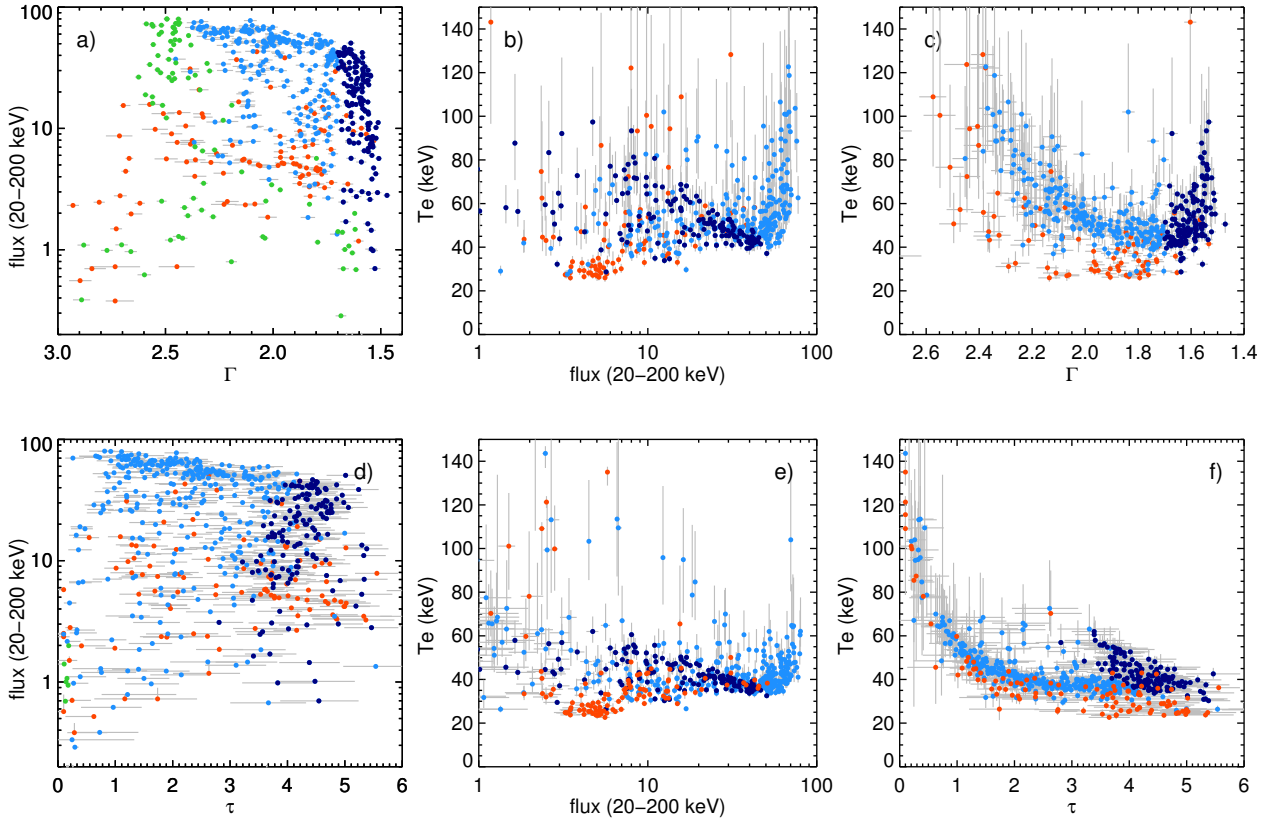**Fig. 4.** Relations between the parameters derived from our spectral fits, via the NTHCOMP (panels **a)**–**c)**) and COMPPS models (panels **d)**–**f)**). Green, blue and red symbols are used to highlight the best-fitting model, according to our model selection criteria (Sect. 2.2). Blue: comptonization models with constrained T_e (Fig. 1a) further divided into hard ($\Gamma \leq 1.7$; dark blue) and soft spectra ($\Gamma > 1.7$; light blue). Green: Comptonization models with unconstrained T_e (Fig. 1b). Red: p–value <0.05 fits. (Fig. 1c). Panel **a)** $F_x - \Gamma$ diagram. We find a hard branch (dark blue points) where F_x and Γ are correlated, similar to the hard state in the BHB HID. At the highest fluxes in the outburst, we find the soft flaring branch (light blue points), similar to the BHB HID intermediate states. We also identify the softest spectra in our sample ($\Gamma \gtrsim 2.4$) with unconstrained T_e with a tentative ultra-luminous state (green points). The different branches also occupy characteristic regions in panel **d)** $F_x - \tau$ diagram, panels **b)**, **e)**, $F_x - T_e$ diagrams, panel **c)** $\Gamma - T_e$ diagram and panel **f)** $\tau - T_e$ diagram. The various parameter correlations are described in detail in Sect. 3.3.

model better describing the data. Also, the p–value of the fit with respect to the data was verified in these new fits.

For the spectra obtained during the X-ray plateaus, the ΔBIC model selection criterium favours a Comptonized model with N_H values in excess of the interstellar one ($N_H \gtrsim 5 \times 10^{24}$ cm^{-2}; see Figs. 5, 6) regardless of whether reflection is considered or not. However, N_H is constrained better when no reflection is considered (see Fig. 5). The validity of the models is supported by the p–value of the fit with respect to the data, which is now p–value ≥ 0.05 for the fits to the plateau spectra when the absorption is left to vary freely, with or without reflection. During X-ray flares, the BIC model selection favours a Comptonized model where the absorption is fixed to the interstellar values. The energy range analysed in this work (20–200 keV) only allows firm constraints on the most extreme N_H values ($N_H \gtrsim 5 \times 10^{24}$ cm^{-2}). Although we observe an evolution of the derived N_H values in anti-correlation with the flux evolution (i.e. N_H reaches the highest values during the X-ray plateaus and decreases during the X-ray flares).

Using solely the 20–200 keV energy range of our spectra, we cannot simultaneously constrain N_H and the reflection contribution to the source spectra (quantified using the R parameter in COMPPS, Fig. 6e), as shown by the large uncertainties in the determination of both parameters (Figs. 6d, e). The BIC model selection criterium favours a Comptonized model with variable column density over a Comptonized model with variable column

density and variable reflection. Only by extending the fitting range to lower energies we will be able to model simultaneously the absorption and reflection parameters in our fits.

Finally, we note that with the spectral fits presented in this section, the peculiar increase of τ, and simultaneous decrease of T_e derived during the X-ray plateaus largely disappears, (see Figs. 2, 5, 6) suggesting that the systematic changes of these parameters were the result of inaccurate modelling.

4. Discussion

The light curve of V404 Cyg during the June 2015 outburst does not display the typical features of the standard BHB light curves (e.g. Chen et al. 1997; Remillard & McClintock 2006). Similarly, the soft X-ray spectra of V404 Cyg are remarkably different from the spectra of other BHBs, mostly owing to extreme intrinsic absorption (Motta et al. 2017) also seen in the 1989 outburst (Życki et al. 1999). However, when we look at the source spectra in hard X-rays (above 20 keV), we find some similarities between V404 Cyg and other BHBs.

4.1. Hard branch

We have identified a hard branch in the $F_X - \Gamma$ diagram of V404 Cyg that is reminiscent of the hard state branch of the
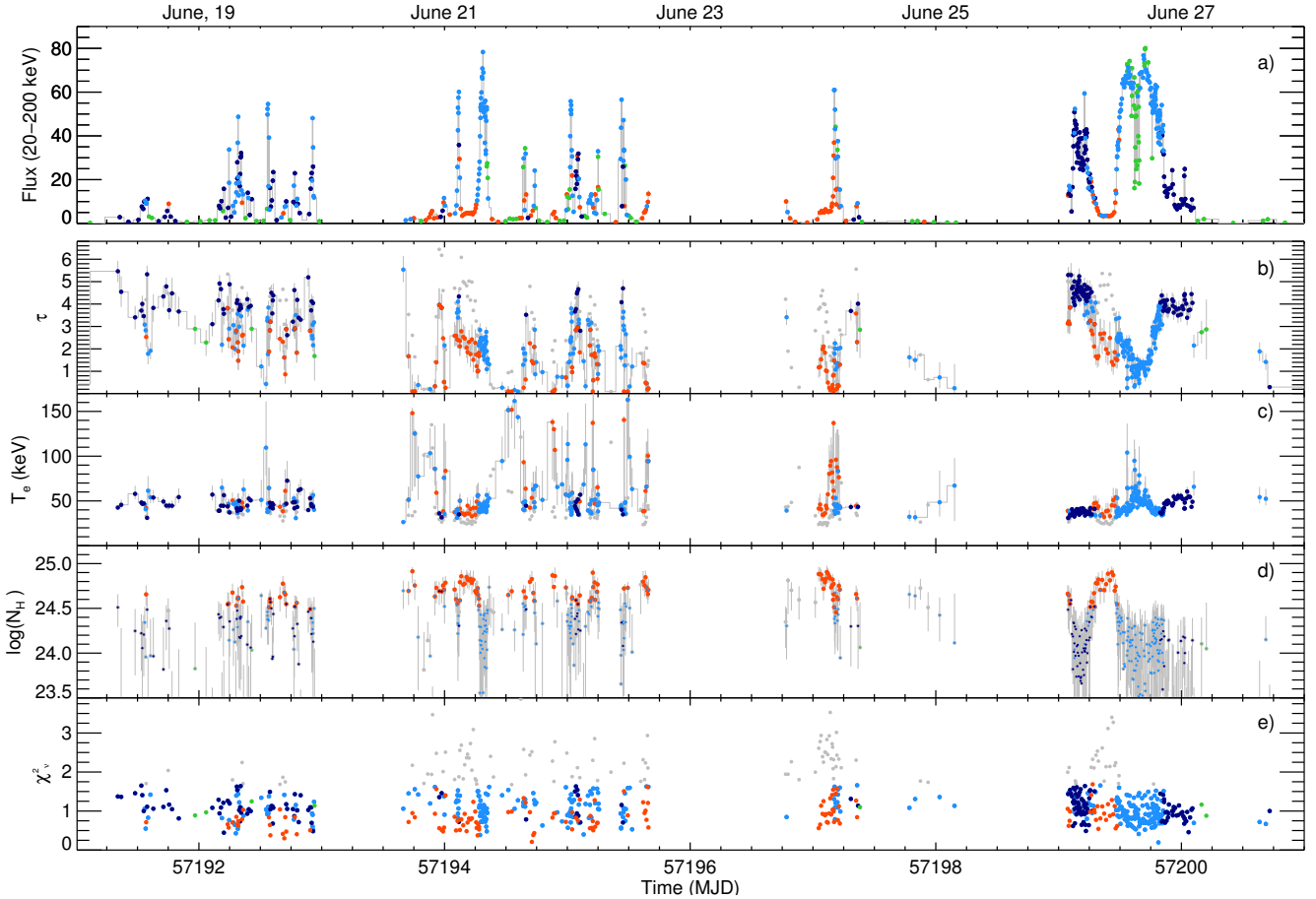
Fig. 5. Time evolution of the flux and spectral parameters of V404 Cyg during the June 2015 flaring episodes. Green and blue symbols are unchanged with respect to Fig. 2. Red symbols highlight the parameters obtained fitting the data with a Comptonized model (COMPPS) modified by variable absorption. The BIC model selection (see text) favours this model only for the spectra detected during the X-ray plateaus. For comparison, we also show the parameters obtained in the fits to these spectra fixing the absorption to interstellar values (grey symbols in panels **b)**, **c)** and **e)**. Panel **a)** source flux (20–200 keV) in units of 10^{-8} erg cm^{-2} s^{-1}. Panel **b)** optical depth, τ, Panel **c)** electron temperature, T_e. Panel **d)** N_H values obtained for the whole data set when leaving N_H as a free parameter; only when $N_H \gtrsim 10^{24}$ cm^{-2} modifies substantially the spectral shape in the IBIS/ISGRI energy range, can this value be properly constrained in our spectral fits. This happens during the X-ray plateaus. Panel **e)** χ^2_ν value for every fit.

BHB HID (Homan et al. 2001; Belloni 2004; Fender et al. 2004; Dunn et al. 2010; Belloni & Motta 2016). The hard branch is occupied by the hardest spectra in our sample ($\Gamma \leq 1.7$). In the hard branch, the spectrum of V404 Cyg gradually softens and T_e decreases from $T_e \sim 80$ keV or unconstrained (NTHCOMP) down to about $T_e \sim 40$ keV as the flux increases (Fig. 4a, d, b, e). This F_x–T_e anti-correlation has been observed by Natalucci et al. (2015) and Roques et al. (2015) in the analysis of IBIS/ISGRI and SPI data obtained during rev. 1554 (EPOCH 1) and by Jenke et al. (2016) using *Fermi*/GBM data. Similar anti-correlations have also been found in other BHBs in the hard state (Esin et al. 1998; Wardziński et al. 2002; Rodriguez et al. 2003; Motta et al. 2009; Kajava et al. 2016), supporting our identification of the hard branch with the hard state of prototypical BHBs (Belloni & Motta 2016). The F_x–T_e anti-correlation in the hard branch can be explained by the truncated disk/hot inner flow model (Esin et al. 1997; Mayer & Pringle 2007), which assumes that at low luminosities the accretion disk is truncated at distances between a few tens and a few thousand gravitational radii from the BH, and only a small fraction of disk photons reach the hot flow/comptonizing medium. The X-ray spectrum would then be produced by pure synchrotron self-Compton emission (SSC) in an hybrid (thermal

plus non-thermal) Comptonizing medium (Poutanen & Vurm 2009; Malzac & Belmont 2009; Veledina et al. 2011). V404 Cyg may be in this regime at fluxes below $\sim 10^{-8}$ erg cm^{-2} s^{-1}, where we measure T_e in the range 60–80 keV (or unconstrained). As the accretion rate increases, the inner radius of the accretion disk moves inwards, closer to the BH, and a growing number of soft seed photons from the accretion disk enter the Comptonizing medium, gradually cooling down the population of thermal electrons (Poutanen & Vurm 2009; Malzac & Belmont 2009; Veledina et al. 2011). Electron cooling results in softer Comptonized spectra (Done et al. 2007). The electron cooling could cause the observed F_x–T_e anti-correlation and gradual spectral softening in the hard branch. Observations of GX 339–4 (Wardziński et al. 2002) and GRO J1655–40 (Joinet et al. 2008) in the hard state result in T_e values that are comparable to our measurements. However, these systems displayed lower τ values ($\tau \approx 2.5$) than those measured for V404 Cyg ($\tau \approx [3$–$5.5]$) which suggests that we are dealing with an optically thicker Comptonizing medium. The τ values we derive are comparable to those found during the 1989 outburst of V404 Cyg ($\tau \approx 6$; Życki et al. 1999). As the optical depth is expected to scale linearly with the mass accretion rate (Różańska & Czerny 2000), the presence of an optically thick Comptonizing medium may
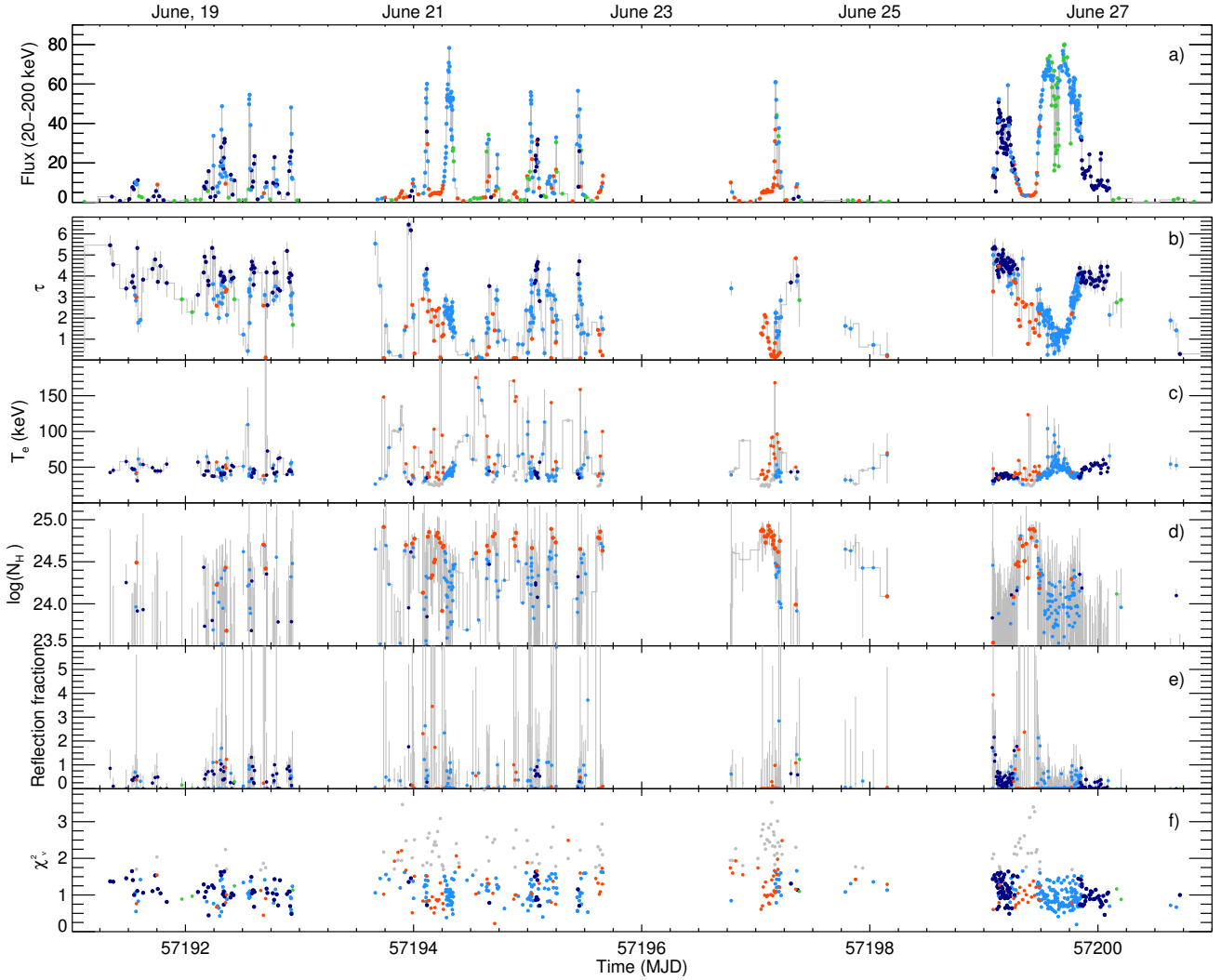
Fig. 6. Same as Fig. 5, but for a Comptonized model (COMPPS) modified by variable absorption and reflection. Panel **a)** source flux (20–200 keV) in units of 10^{-8} erg cm^{-2} s^{-1}. Panel **b)** optical depth, τ, Panel **c)** electron temperature, T_e. Panel **d)** N_H values obtained for the whole data set when leaving N_H as a free parameter. Panel **e)** Reflection fraction (Parameter R in COMPPS). Panel **f)** χ^2_ν value for each fit.

be connected to V404 Cyg emitting closer to the Eddington limit than other BHBs in the hard state.

4.2. Soft flaring branch

In the soft flaring branch the spectrum still softens as the flux increases, but most of the parameter dependencies are reversed with respect to the hard branch, suggesting a change in the hard X-ray production mechanism: as F_x increases, the optical depth of the Comptonizing medium decreases and the spectrum softens (Fig. 4c), while the electron temperature increases (Fig. 4b, e). These parameter relations are similar to those observed during hard to soft state transitions in other BHBs (Phlips et al. 1996; Esin et al. 1998; Joinet et al. 2008; Motta et al. 2009; Del Santo et al. 2013), suggesting that the soft flaring branch may correspond to the BHB intermediate state. The decrease in τ observed during hard to soft state transitions is consistent with the material in the Comptonizing medium condensing into a disk, or being ejected into an outflow (Malzac 2016). The detection of a cut-off in the spectrum is indicative of a significant fraction of thermal electrons in the Comptonizing medium. The parameter Te increases as the flux progressively

increases, suggesting that the injection of external (disk) photons, which cooled down the electron cloud in the hard branch might have ceased or its cooling effect on the electron cloud is negligible.

The steepest spectra in our sample with $\Gamma \gtrsim 2.4$ (or $\tau \lesssim 1.0$) are those where T_e is not constrained (NTHCOMP). Fits to these data using COMPPS provide extremely low τ and high T_e values. When the optical depth is low, the particles do not have time to thermalize between re-accelerations, and the electron distribution resembles the power-law injection function that could originate from magnetic reconnection or shock acceleration (Veledina et al. 2011; Del Santo et al. 2013). These spectra are detected at epochs bracketed by the largest measured T_e values ($\gtrsim$80 keV), so it is likely that they are caused by the electron population becoming simultaneously hotter and/or progressively less thermal. When detected at the highest fluxes ($\gtrsim$20 × 10^{-8} erg cm^{-2} s^{-1}), the $\Gamma \gtrsim 2.4$ spectra occupy a region in the F_x−Γ diagram (Fig. 4a) that is reminiscent of the HID ultra-luminous state (Dunn et al. 2010), which suggests that these spectra could be analogous to the ultra-luminous state of GX 339-4 (Miyamoto et al. 1991; Kubota & Done 2016), GS 1124–68

([Miyamoto et al. 1993](#)), XTE J1550–564 ([Sobczak et al. 1999b](#); [Kubota & Makishima 2004](#); [Hjalmarsdotter et al. 2016](#)), GRO J1655–40 ([Sobczak et al. 1999a](#); [Joinet et al. 2008](#)), or 4U 1630–47 ([Abe et al. 2005](#)). In such a state the spectrum is a composite of a strong disk and a steep prominent Comptonized tail, with no cut-off at high energies, which may extend up to ~ 1 MeV ([Kubota & Done 2016](#)).

When detected at the lowest fluxes, these $\Gamma \gtrsim 2.4$ spectra could be analogous to the soft state spectra of some BHB where faint non-thermal hard X-ray tails are detected ([Zdziarski et al. 2017](#)).

4.3. X-ray plateaus

We have observed X-ray plateaus characterized by roughly constant fluxes ($F_x \sim 5 \times 10^{-8}$ erg cm^{-2} s^{-1}) during periods lasting several hours. Often the plateaus are observed in between two or several flares (see Figs. 2, A.1). Furthermore, we only detect X-ray plateaus in epochs 2 and 3, when the source is predominantly in the soft flaring branch, where the spectrum is softer ($\Gamma > 1.7$). We observed that the statistically worse fits ($\chi^2_\nu > 1.8$; see Fig. 2) tend to happen during these X-ray plateaus if we fix N_H to the interstellar value in the direction of the source. The statistics are improved when allowing N_H to vary in our fits ($\chi^2_\nu \sim 1$; see Figs. 5, 6). In this case we derive N_H values ($N_H \gtrsim 5 \times 10^{24}$ cm^{-2}) two orders of magnitude in excess of the interstellar N_H value in the direction of the source ($N_H \sim 0.8 \times 10^{22}$ cm^{-2}), which suggests that intrinsic absorption by Compton-thick material distorts the source spectrum and results in the spectral shape observed during the X-ray plateaus (see Fig. 1c). Owing to the limited energy range available for this analysis, our fits cannot constrain simultaneously N_H and the fraction of X-ray photons reprocessed by the Compton-thick material contributing to the source spectra (i.e. the reflection fraction in COMPPS). Also, if N_H is allowed to vary in our fits, the spectral parameters T_e and τ display values that are consistent with measurements during nearly contemporaneous flares.

In previous studies, [Natalucci et al. (2015)](#), [Roques et al. (2015)](#), and [Jenke et al. (2016)](#) inferred very high seed photon temperatures ~ 6–7 keV, which they attributed to the jet. Our results show that the source spectra can also be modelled using lower seed photons temperatures (consistent with Swift/XRT results; [Motta et al. 2017](#)) and strong local absorption.

4.4. Flaring activity

Although N_H cannot be properly constrained during the X-ray flares, when lower N_H values are derived, N_H is seen to vary in anti-correlation with the evolving X-ray flux over the whole data set analysed here (Fig. 5c). The fact that we derive $N_H \sim 5 \times 10^{24}$ cm^{-2} only during the X-ray plateaus, and clearly lower N_H values in the adjacent flares, suggests that the dramatic intensity drops observed during these plateaus may be partially caused by obscuration of the central source. The obscuring material can be some outflowing material, the outer regions of a Compton-thick accretion disk, or a combination of both. Thus, the apparent flaring activity may actually be the result of a clumpy Compton-thick obscuring material becoming occasionally Compton-thin and allowing the source photons to reach the observer. The fast flare rise and decay times (≈ 30 min, see Fig. A.1) may actually be related to varying partial obscuration of the central source, as previously suggested by [Życki et al. (1999)](#), who measured N_H variability on timescales of minutes during the 1989 outburst.

Perhaps also for the same reason we find a lot of scatter in the correlations between F_x and the source spectral parameters (Γ, τ, T_e), while there is much less scatter in the various parameter correlations (Γ–T_e, τ–T_e; see Fig. 4).

5. Summary of results and conclusions

We have fit the 20–200 keV IBIS/ISGRI spectra of V404 Cyg during the June 2015 outburst using two thermal Comptonization models (NTHCOMP and COMPPS). For the first time we continuously measured the evolution of the properties of the Comptonizing medium during an outburst rise and decay. We find that the system evolves through the same Γ–T_e, τ–T_e and F_x–T_e paths when the outburst rises or decays. We identified two clear spectral branches in the F_x–Γ diagram, which display characteristic parameter relations: a hard branch and a soft flaring branch.

In the hard branch, V404 Cyg shows a hard ($\Gamma \leq 1.7$) thermal Comptonized spectrum, which slowly softens as the flux increases. In the hard branch, τ is correlated with F_x while T_e is anti-correlated with F_x and Γ. Similar parameter correlations have been observed in other BHBs in the hard state, suggesting that the hard branch could correspond to the HID hard state. The observed parameter evolution can be explained in terms of thermal Comptonization of soft seed photons by a hot electron cloud in the vicinity of the BH. The F_x–T_e anti-correlation could result from the electron population progressively cooling down as the accretion disk moves closer to the BH and more disk photons enter the Comptonizing medium.

In the soft flaring branch V404 Cyg shows a soft, thermal Comptonized spectrum, ($\Gamma > 1.7$), which softens as the flux increases. In the soft flaring branch T_e and F_x are correlated, while F_x and τ are anti-correlated. The parameter correlations are consistent with those observed during hard to soft state transitions in other sources, suggesting that these data could correspond to the intermediate state or occasionally the ultra-luminous state. The observed T_e–F_x correlation is compatible with the predictions of SSC-models.

We also found a plateau branch where Comptonization models fail to describe the source spectra if N_H is fixed to the interstellar values in the direction of the source. The fits to these spectra improve when we leave the absorption to vary freely. In this case we derive N_H values ($N_H \gtrsim 5 \times 10^{24}$ cm^{-2}) which suggest that intrinsic absorption by Compton-thick material results in the spectral shape observed during the X-ray plateaus. The obscuring material can be some outflowing material, a clumpy Compton-thick accretion disk, or a combination of both. Thus, we propose that the observed dramatic flaring activity seen at hard X-rays may not only be due to intrinsic source variability, but can partly result from obscuration of the central source by Compton-thick material. The system inclination of 67° may be a key parameter in the observation of such phenomenology that is not observed in other sources seen at lower or higher inclination angles.

References

Abe, Y., Fukazawa, Y., Kubota, A., Kasama, D., & Makishima, K. 2005, [PASJ, 57, 629](#)

Arnaud, K. A. 1996, in Astronomical Data Analysis Software and Systems V, eds. G. H. Jacoby, & J. Barnes, [ASP Conf. Ser., 101, 17](#)

Barthelmy, S. D., & Sbarufatti, B. 2015, GRB Coordinates Network, 17963
Belloni, T. 2004, Nucl. Phys. B Proc. Suppl., 132, 337
Belloni, T. M., & Motta, S. E. 2016, in Astrophysics of Black Holes: From Fundamental Aspects to Latest Developments, ed. C. Bambi, Astrophys. Space Sci. Libr., 440, 61
Beloborodov, A. M. 1999, in High Energy Processes in Accreting Black Holes, eds. J. Poutanen, & R. Svensson, ASP Conf. Ser., 161, 295
Casares, J., Charles, P. A., & Naylor, T. 1992, Nature, 355, 614
Chen, W., Shrader, C. R., & Livio, M. 1997, ApJ, 491, 312
Courvoisier, T. J.-L., Walter, R., Beckmann, V., et al. 2003, A&A, 411, L53
Del Santo, M., Malzac, J., Belmont, R., Bouchet, L., & De Cesare, G. 2013, MNRAS, 430, 209
Done, C., Gierliński, M., & Kubota, A. 2007, A&ARv, 15, 1
Droulans, R., Belmont, R., Malzac, J., & Jourdain, E. 2010, ApJ, 717, 1022
Dunn, R. J. H., Fender, R. P., Körding, E. G., Belloni, T., & Cabanac, C. 2010, MNRAS, 403, 61
Ebisawa, K., Ogawa, M., Aoki, T., et al. 1994, PASJ, 46, 375
Eikenberry, S. S., Dallilar, Y., Garner, A., et al. 2016, AAS/High Energy Astrophysics Division, HEAD Meeting 15, 109.01
Esin, A. A., McClintock, J. E., & Narayan, R. 1997, ApJ, 489, 865
Esin, A. A., Narayan, R., Cui, W., Grove, J. E., & Zhang, S.-N. 1998, ApJ, 505, 854
Fender, R. P., Belloni, T. M., & Gallo, E. 2004, MNRAS, 355, 1105
Ferrigno, C., Bozzo, E., Boissay, R., Kuulkers, E., & Kretschmar, P. 2015, ATel, 7731
Gandhi, P., Littlefair, S. P., Hardy, L. K., et al. 2016, MNRAS, 459, 554
Gierliński, M., Zdziarski, A. A., Poutanen, J., et al. 1999, MNRAS, 309, 496
Hjalmarsdotter, L., Axelsson, M., & Done, C. 2016, MNRAS, 456, 4354
Homan, J., Wijnands, R., van der Klis, M., et al. 2001, ApJS, 132, 377
Jenke, P. A., Wilson-Hodge, C. A., Homan, J., et al. 2016, ApJ, 826, 37
Joinet, A., Jourdain, E., Malzac, J., et al. 2007, ApJ, 657, 400
Joinet, A., Kalemci, E., & Senziani, F. 2008, ApJ, 679, 655
Kajava, J. J. E., Veledina, A., Tsygankov, S., & Neustroev, V. 2016, A&A, 591, A66
Kass, R., & Raftery, A. 1995, Journal of the American Statistical Association, 90, 773
Khargharia, J., Froning, C. S., & Robinson, E. L. 2010, ApJ, 716, 1105
Kimura, M., Isogai, K., Kato, T., et al. 2016, Nature, 529, 54
Kubota, A., & Done, C. 2016, MNRAS, 458, 4238
Kubota, A., & Makishima, K. 2004, ApJ, 601, 428
Kuulkers, E. 2015, ATel, 7758
Lebrun, F., Leray, J. P., Lavocat, P., et al. 2003, A&A, 411, L141
Loh, A., Corbel, S., Dubus, G., et al. 2016, MNRAS, 462, L111
Makino, F. 1989, IAU Circ., 4782, 1
Malzac, J. 2016, Astron. Nachr., 337, 391
Malzac, J., & Belmont, R. 2009, MNRAS, 392, 570
Malzac, J., Petrucci, P. O., Jourdain, E., et al. 2006, A&A, 448, 1125
Marsden, B. G. 1989, IAU Circ., 4783
Mayer, M., & Pringle, J. E. 2007, MNRAS, 376, 435
McConnell, M. L., Zdziarski, A. A., Bennett, K., et al. 2002, ApJ, 572, 984
Miller-Jones, J. C. A., Jonker, P. G., Dhawan, V., et al. 2009, ApJ, 706, L230

Miyamoto, S., Kimura, K., Kitamoto, S., Dotani, T., & Ebisawa, K. 1991, ApJ, 383, 784
Miyamoto, S., Iga, S., Kitamoto, S., & Kamado, Y. 1993, ApJ, 403, L39
Motta, S., Belloni, T., & Homan, J. 2009, MNRAS, 400, 1603
Motta, S., Homan, J., Muñoz Darias, T., et al. 2012, MNRAS, 427, 595
Motta, S. E., Belloni, T. M., Stella, L., Muñoz-Darias, T., & Fender, R. 2014, MNRAS, 437, 2554
Motta, S. E., Kajava, J. J. E., Sánchez-Fernández, C., Giustini, M., & Kuulkers, E. 2017, MNRAS, 468, 981
Muñoz-Darias, T., Casares, J., Mata Sánchez, D., et al. 2016, Nature, 534, 75
Murphy, K. D., & Yaqoob, T. 2009, MNRAS, 397, 1549
Narayan, R., & Yi, I. 1995, ApJ, 452, 710
Natalucci, L., Fiocchi, M., Bazzano, A., et al. 2015, ApJ, 813, L21
Negoro, H., Matsumitsu, T., Mihara, T., et al. 2015, ATel, 7646
Oosterbroek, T., van der Klis, M., Vaughan, B., et al. 1996, A&A, 309, 781
Phlips, B. F., Jung, G. V., Leising, M. D., et al. 1996, ApJ, 465, 907
Poutanen, J., & Svensson, R. 1996, ApJ, 470, 249
Poutanen, J., & Veledina, A. 2014, Space Sci. Rev., 183, 61
Poutanen, J., & Vurm, I. 2009, ApJ, 690, L97
Remillard, R. A., & McClintock, J. E. 2006, ARA&A, 44, 49
Richter, G. A. 1989, Information Bulletin on Variable Stars, 3362
Rodriguez, J., Corbel, S., & Tomsick, J. A. 2003, ApJ, 595, 1032
Rodriguez, J., Cadolle Bel, M., Alfonso-Garzón, J., et al. 2015, A&A, 581, L9
Roques, J.-P., Jourdain, E., Bazzano, A., et al. 2015, ApJ, 813, L22
Różańska, A., & Czerny, B. 2000, A&A, 360, 1170
Schwarz, G. 1978, Annals of statistics, 6, 461
Segreto, A., Del Santo, M., D'Aí, A., et al. 2015, ATel, 7755
Shakura, N. I., & Sunyaev, R. A. 1973, A&A, 24, 337
Shapiro, S. L., Lightman, A. P., & Eardley, D. M. 1976, ApJ, 204, 187
Siegert, T., Diehl, R., Greiner, J., et al. 2016, Nature, 531, 341
Sivakoff, G. R., Bahramian, A., Altamirano, D., et al. 2015, ATel, 7959
Sobczak, G. J., McClintock, J. E., Remillard, R. A., Bailyn, C. D., & Orosz, J. A. 1999a, ApJ, 520, 776
Sobczak, G. J., McClintock, J. E., Remillard, R. A., et al. 1999b, ApJ, 517, L121
Sunyaev, R. A., & Truemper, J. 1979, Nature, 279, 506
Tanaka, Y. 1989, in Two Topics in X-Ray Astronomy, Volume 1: X Ray Binaries. Volume 2: AGN and the X Ray Background, eds. J. Hunt, & B. Battrick, ESA SP, 296
Tetarenko, A., Sivakoff, G. R., Young, K., Wouterloot, J. G. A., & Miller-Jones, J. C. 2015, ATel, 7708
Veledina, A., Vurm, I., & Poutanen, J. 2011, MNRAS, 414, 3330
Walton, D., Harrison, F., Forster, K., et al. 2015, ATel, 7752
Walton, D. E. 2016, AAS/High Energy Astrophysics Division, 15, 109.08
Wardziński, G., Zdziarski, A. A., Gierliński, M., et al. 2002, MNRAS, 337, 829
Winkler, C., Courvoisier, T. J.-L., Di Cocco, G., et al. 2003, A&A, 411, L1
Younes, G. 2015, GRB Coordinates Network, 17932
Zdziarski, A. A., Johnson, W. N., & Magdziarz, P. 1996, MNRAS, 283, 193
Zdziarski, A. A., Lubiński, P., & Sikora, M. 2012, MNRAS, 423, 663
Zdziarski, A. A., Malyshev, D., Chernyakova, M., & Pooley, G. G. 2017, MNRAS, submitted
Życki, P. T., Done, C., & Smith, D. A. 1999, MNRAS, 309, 561

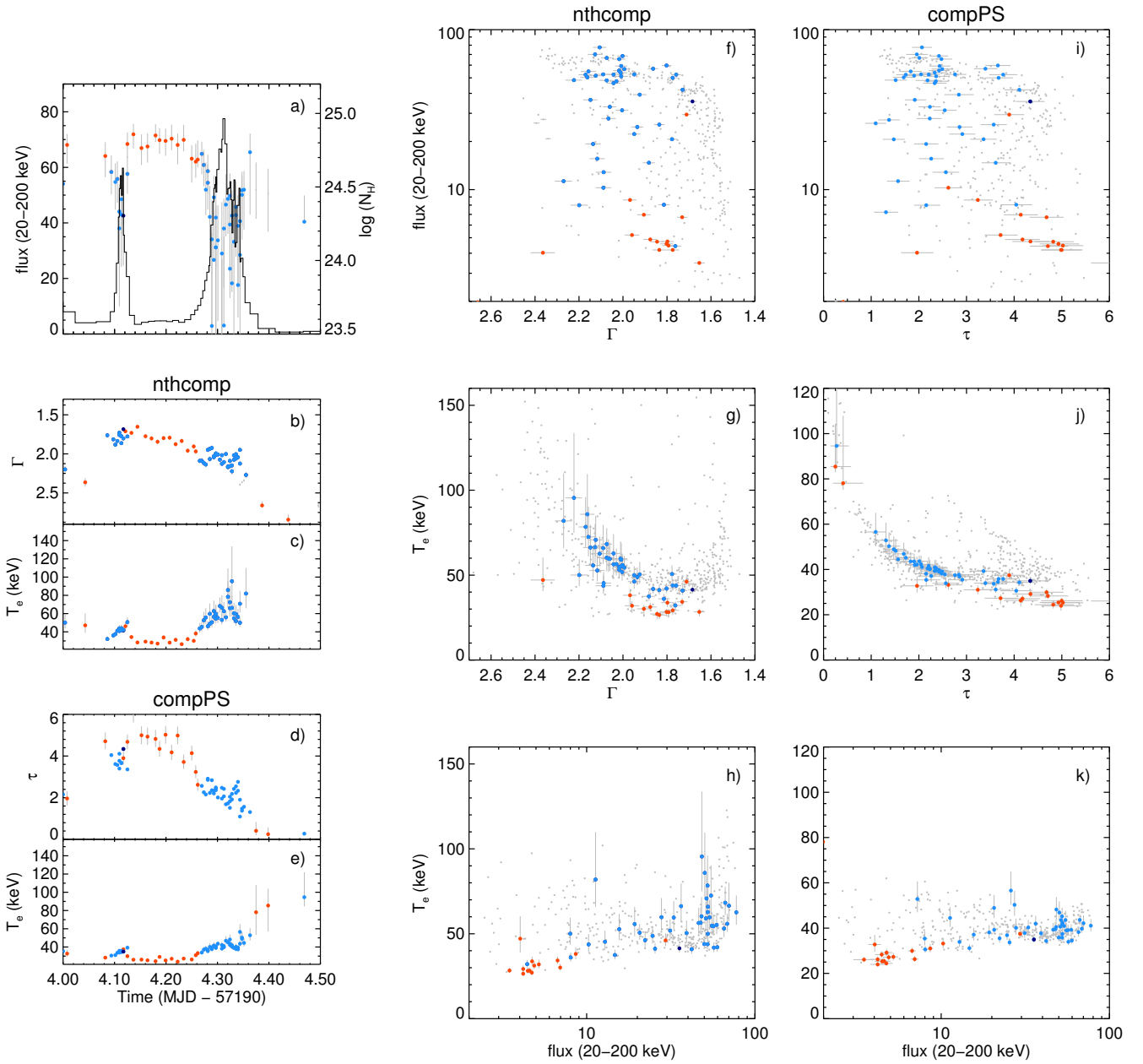## Appendix A: Closer view to some flares

Fig. A.1. Close view of the properties of the X-ray plateau detected on MJD 57 194.0–57 194.4, derived fitting the source spectra with Comptonization models (NTHCOMP and COMPPS). Panel **a)** time evolution of the source flux, F_x, in the 20–200 keV energy range ($\times 10^{-8}$ erg cm^{-2} s^{-1}) in comparison with the N_H evolution, where N_H was derived by leaving it as a free parameter in our fits, as described in Sect. 3.4. The plateau was characterized by a roughly constant flux $F_x \sim 5 \times 10^{-8}$ erg cm^{-2} s^{-1} and was interrupted by two big flares around MJD 57 194.1 and 57 194.3 with peak fluxes of $F_x \sim 60$ and 80×10^{-8} erg cm^{-2} s^{-1}. We observed roughly constant N_H values during the X-ray plateau ($N_H \sim 5 \times 10^{24}$ cm^{-2}). Systematically lower N_H values were measured during the two X-ray flares. However, N_H cannot be properly constrained by our fits to the flare spectra. Panels **b)–e)** time evolution of the spectral parameters derived for this period. Panels **f)–h)** relations between the various NTHCOMP spectral parameters during this period. Panels **i)–k)** relations between the various COMPPS spectral parameters during this period. For reference, we also show in panels **f)–k)** the complete dataset analysed in this work (grey points). The parameters derived during the peaks of the flares occupy the soft flaring branch, (see Sect. 3.3), while the flare rise and decays, which are likely affected by partial obscuration, occupy intermediate regions between the soft flaring branch and the plateau branch in the panels **f)** and **i)**.
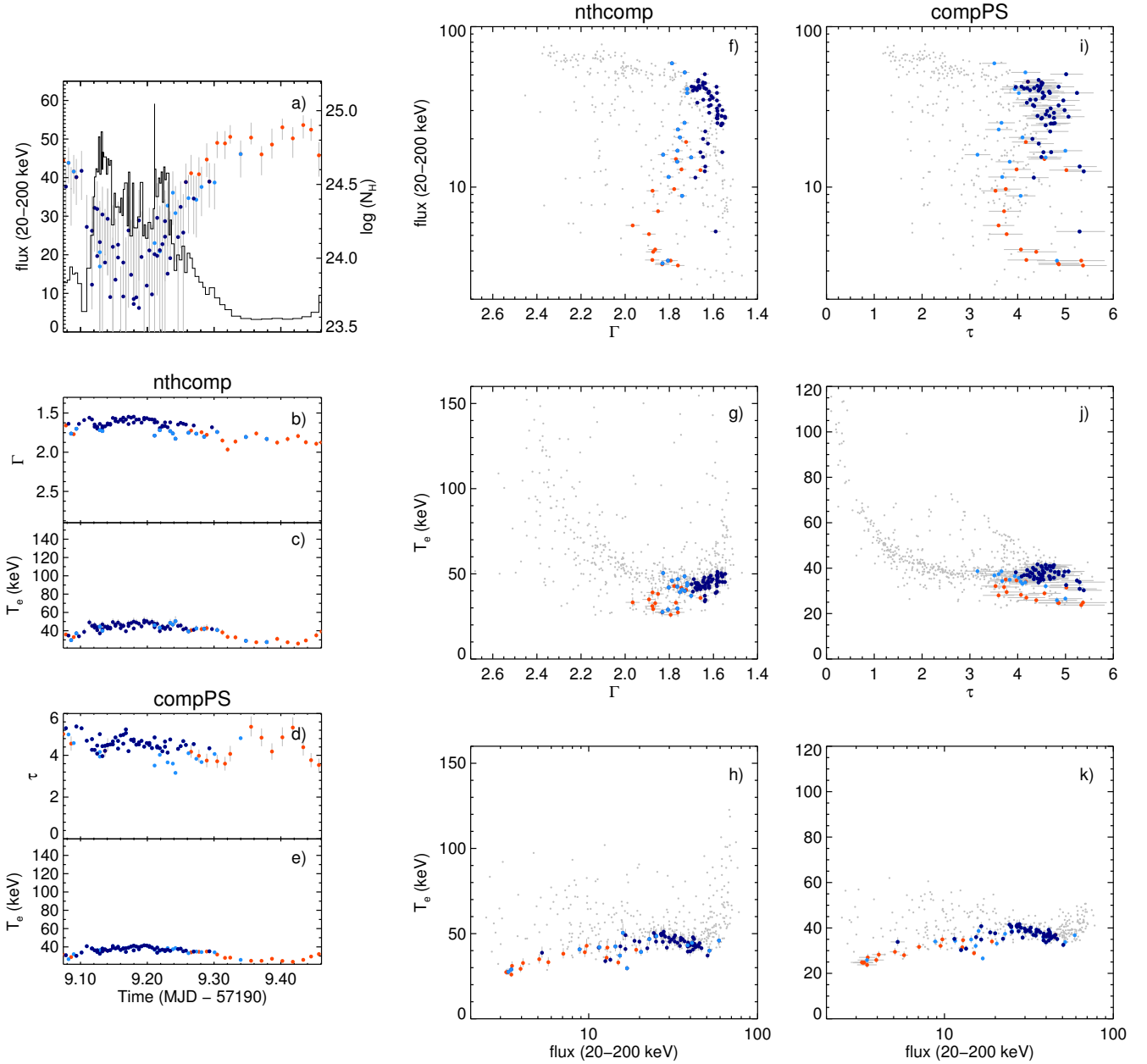
Fig. A.2. Close view of the properties of the hard X-ray flare and subsequent X-ray plateau detected around MJD 55 199, derived fitting the source spectra with Comptonization models (NTHCOMP and COMPPS). Panel **a)** time evolution of the source flux, F_x, in the 20–200 keV energy range ($\times 10^{-8}$ erg cm^{-2} s^{-1}) in comparison with the N_H evolution, where N_H is derived by leaving it as a free parameter in our fits, as described in Sect. 3.4. During the peak of the flare, when N_H displays lower values, it cannot be constrained by our fits. Panels **b)**–**e)** time evolution of the spectral parameters derived for this period. Panels **f)**–**h)** relations between the various NTHCOMP spectral parameters during this period. Panels **i)**–**k)** relations between the various COMPPS spectral parameters during this period. For reference, we also show in panels **f)**–**k)** the complete dataset analysed in this work (grey points). In the diagrams in panels **f)**–**k)** we observe parameter correlations characteristic of the hard branch (see sect. 3.3). The dramatic changes in flux observed during this X-ray flare are accompanied by little variations in Γ and τ. Brief transitions to the soft flaring branch are observed during the peak of the flare. During the flare decay, the spectrum gradually softens, T_e decreases and τ displays high variability, while we observe a gradual increase in N_H, which reaches values close to 10^{25} cm^{-2} when the system reaches the bottom of the X-ray plateau. The spectral parameters derived during the X-ray plateau, occupy a separate region, as is evident in panels **f)**–**h)**. Also, the parameter correlations reverse in the plateau branch with respect to the trends observed in the hard branch.
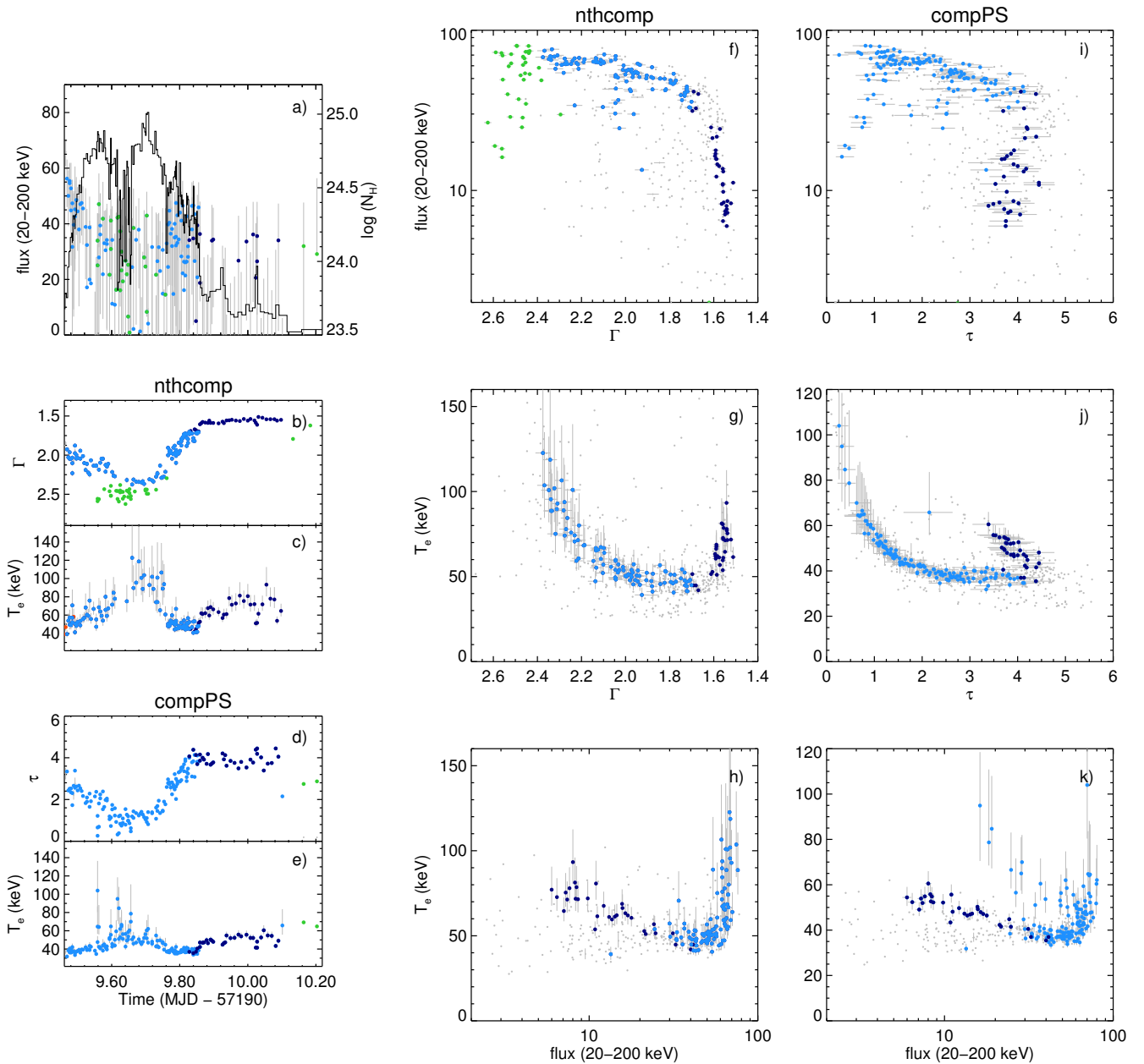
Fig. A.3. Close view of the properties of the soft X-ray flare detected around MJD 57 200, derived fitting the source spectra with Comptonization models (NTHCOMP and COMPPS). Panel **a)** time evolution of the source flux, F_x, in the 20–200 keV energy range ($\times 10^{-8}$ erg cm^{-2} s^{-1}) in comparison with the N_H evolution, where N_H was derived by leaving it as a free parameter in our fits, as described in Sect. 3.4. During the flare, when N_H displayed lower values, it could not be constrained by our fits. Panels **b)–e)** time evolution of the spectral parameters derived for this period. Panels **f)–h)** relations between the various NTHCOMP spectral parameters during this period. Panels **i)–k)** relations between the various COMPPS spectral parameters during this period. For reference, we also show in panels **f)–k)** the complete dataset analysed in this work (grey points). During the flare rise and decay we observed parameter correlations characteristic of the soft flaring branch (see panels **f)–k)**, Sect. 3.3). Around the peak of the flare, the spectra softened above $\Gamma \sim 2.4$ and T_e was constrained using NTHCOMP. Spectral fits to these data using COMPPS provided un-constrained T_e values ($T_e \gtrsim 100$ keV), and the lowest τ values found in this work ($\tau \lesssim 1$). These spectra occupy a region in the Γ–F_x diagram (panel **f)**) reminiscent of the ultra-luminous state in the BHB HID. These spectra also occupy a separate branch in the COMPPS F_x–T_e diagram (panel **i)**). After the peak of the flare, as F_x decreased and the spectrum hardened below $\Gamma \sim 2.4$ the system returned to the soft flaring branch. Around MJD 57 199.85 a dramatic drop in flux was observed (from $F_x \sim 50$ to $F_x \sim 15 \times 10^{-8}$ erg cm^{-2} s^{-1} in about half an hour) and the system entered the hard branch. After this transition, the system started the decay to quiescence, following the hard branch characteristic correlations, but for a decreasing flux.